

Iron Oxide Nanoparticles Induce Dopaminergic Damage: In vitro Pathways and In Vivo Imaging Reveals Mechanism of Neuronal Damage

Syed Z. Imam¹ · Susan M. Lantz-McPeak¹ · Elvis Cuevas¹ · Hector Rosas-Hernandez¹ · Serguei Liachenko¹ · Yongbin Zhang² · Sumit Sarkar¹ · Jaivijay Ramu¹ · Bonnie L. Robinson¹ · Yvonne Jones² · Bobby Gough¹ · Merle G. Paule¹ · Syed F. Ali¹ · Zbigniew K. Binienda¹

Published online: 23 June 2015

© Springer Science+Business Media New York (outside the USA) 2015

Abstract Various iron-oxide nanoparticles have been in use for a long time as therapeutic and imaging agents and for supplemental delivery in cases of iron-deficiency. While all of these products have a specified size range of ~40 nm and above, efforts are underway to produce smaller particles, down to ~1 nm. Here, we show that after a 24-h exposure of SHSY-5Y human neuroblastoma cells to 10 µg/ml of 10 and 30 nm ferric oxide nanoparticles (Fe-NPs), cellular dopamine content was depleted by 68 and 52 %, respectively. Increases in activated tyrosine kinase c-Abl, a molecular switch induced by oxidative stress, and neuronal α -synuclein expression, a protein marker associated with neuronal injury, were also observed (55 and 38 % percent increases, respectively). Inhibition of cell-proliferation, significant reductions in the number of active mitochondria, and a dose-dependent increase in reactive oxygen species (ROS) were observed in neuronal cells. Additionally, using a rat in vitro blood–brain barrier (BBB) model, a dose-dependent increase in ROS accompanied by increased fluorescein efflux demonstrated compromised BBB integrity.

Susan M. Lantz-McPeak and Elvis Cuevas contributed equally to this work.

Electronic supplementary material The online version of this article (doi:10.1007/s12035-015-9259-2) contains supplementary material, which is available to authorized users.

✉ Syed Z. Imam
Syed.Imam@fda.hhs.gov

✉ Zbigniew K. Binienda
Zbigniew.Binienda@fda.hhs.gov

¹ Division of Neurotoxicology, US FDA/National Center for Toxicological Research, Jefferson, AR, USA

² NCTR/ORANanotechnology Core Facility, US FDA/National Center for Toxicological Research, Jefferson, AR, USA

To assess translational implications, in vivo Fe-NP-induced neurotoxicity was determined using in vivo MRI and post-mortem neurochemical and neuropathological correlates in adult male rats after exposure to 50 mg/kg of 10 nm Fe-NPs. Significant decrease in T_2 values was observed. Dynamic observations suggested transfer and retention of Fe-NPs from brain vasculature into brain ventricles. A significant decrease in striatal dopamine and its metabolites was also observed, and neuropathological correlates provided additional evidence of significant nerve cell body and dopaminergic terminal damage as well as damage to neuronal vasculature after exposure to 10 nm Fe-NPs. These data demonstrate a neurotoxic potential of very small size iron nanoparticles and suggest that use of these ferric oxide nanoparticles may result in neurotoxicity, thereby limiting their clinical application.

Keywords Iron-oxide nanoparticles · Fe-NPs · Neuroblastoma cells · Neurotoxicity · Dopamine · Mitochondria · Magnetic resonance imaging

Introduction

Ferric oxide nanoparticles (Fe-NPs) have recently attracted extensive interest due to their superparamagnetic physico-chemical properties and potential biomedical and industrial applications. These applications include brain imaging, brain-targeted drug or gene delivery, catalysis, and magnetic storage [1]. Previous studies have proposed that Fe-NPs could be transported via the olfactory nerve tract to the brain, causing oxidative stress and ultrastructural alterations in olfactory bulb nerve cells [2]. Little is known about the accumulation, retention, and adverse effects of Fe-NPs in the brain. Polymeric coated Fe-NPs formulated to contain Fe(III) and Fe(II) have

been shown to cross the BBB due to their interaction with transferrin, a primary iron-binding protein within the body [3]; so, it is important to assess the potential neurotoxicity of Fe-NPs as their therapeutic use is anticipated to increase. It has been shown that clearance of Fe-NPs requires from 3 to 7 weeks, depending on the size of particles and the coating material. Both can affect bio-distribution and degradation of NPs [3]. Once in biological systems, Fe-NPs may lose their coating, resulting in an accumulation of free iron in brain and other organs that may lead to an increase in ROS production and oxidative stress, subsequently leading to mitochondrial damage and cytotoxicity [4, 5]. The generation of free radicals such as superoxide and nitric oxide leads to the formation of more powerful oxidants like peroxynitrite, which is suggested to be involved in several agent-induced neurotoxicities and neurodegenerative disorders [6]. In addition to our own studies, several reports suggest that oxidative stress can play an important role in damage to dopaminergic systems caused by the substituted amphetamines as well as MPTP [7–12]. Long-term mitochondrial dysfunction also leads to changes in peripheral nervous system integrity as shown in rats exposed to the mitochondrial toxin, 3-nitropropionic acid [13]. Although Fe-NPs-induced cytotoxicity has been studied in PC12 cells [14], the precise cellular pathways and mechanisms associated with that toxicity are not yet well defined. A recent report from the *in vitro* studies has suggested that Fe-NPs decrease neuron viability, trigger oxidative stress, and activate JNK- and p53-mediated pathways to regulate the cell cycle and apoptosis [15]. Findings from another *in vitro* study suggested that NPs induce microglial activation and subsequently cause the release of pro-inflammatory factors that contributed to cellular dysfunction and cytotoxicity in PC12 cells [16]. The present study was conducted to determine if exposure to Fe-NPs activates specific signaling pathways that induce dopaminergic neuronal toxicity in cell cultures of SHSY-5Y human neuroblastoma cells. Our study was further extended to assess the mechanisms of dopaminergic neuronal damage induced by Fe-NPs *in vivo* in adult rats. This study represents the first of its kind to show in real time the transfer of Fe-NPs from the blood stream into brain ventricles and the impact of Fe-NPs on brain volume and chemistry. Additionally, we provide data on possible mechanisms that may underlie the expression of Fe-NPs-induced dopaminergic neuronal damage by assessing the impact of Fe-NPs on the integrity of the BBB, using a rodent brain microvessel endothelial cell model.

Materials and Methods

Fe-NPs Characterization

Fe-NPs used in this study were obtained from Ocean Nanotechnology Inc. (Springdale, AR) and characterized by

manufacture. The physicochemical properties were characterized and validated in FDA Nanotechnology Core Facility in Jefferson Laboratories prior to conducting the biological study. Transmission electron microscopy (TEM) was used to measure the primary size, shape, and morphology of the Fe-NPs. TEM images were collected using a JEM-2100 (JEOL Inc., Peabody, MA.) equipped with a charged coupled device (CCD) camera. The acceleration voltage used for the analyses was 80 kV. The Fe-NPs were homogeneously dispersed (10 µg/ml) in 2-propanol, and 3 µl of the suspension was deposited on a carbon-coated TEM grid, dried, and evacuated before analysis. An energy dispersive X-ray (EDAX) spectral detector (EDS) was used to detect nanomaterials with elemental composition based on X-ray emissions of the material in the electron beam. Energy dispersive X-ray (EDX) elemental analysis was affected with accelerating voltage of 15 kV. The mean and standard deviation (SD) of the particle size was calculated from the measurement of over 100 nanoparticles in random fields of view.

The hydrodynamic diameter and zeta potential of Fe-NPs were measured in water using a Zetasizer Nano ZS (Malvern, Worcestershire, UK) as previously described [17]. Briefly, the Fe-NPs samples were measured after dilution of the nanoparticle stock solution to 50 µg/ml in water. These dilutions were sonicated for 5 min to provide a homogenous dispersion. For the size measurement, 70 µL of the diluted dispersion Fe-NPs was transferred to a cuvette for hydrodynamic size measurement; for zeta potential measurement, a Malvern zeta potential cell was washed three times with ultrapure water followed by transferring 850 µl of diluted dispersion nanoparticles to this cell to measure the zeta potential. Both size and zeta potential were measured at least three times. The data were calculated as the average size or zeta potential of nanoparticles.

Cell Culture Studies

SHSY-5Y human neuroblastoma cells (ATCC Cultures Inc., VA) were cultured in Dulbecco's modified Eagle medium (DMEM) containing 10 % FBS [18]. SH-SY5Y cells were treated with 10 or 30 nm of Fe-NPs (2.5, 5 or 10 µg/ml) or 500 µM methamphetamine (METH) as a positive control for 24 h in medium containing 2 % serum. In some cases, cells were also treated with ferric chloride or ferrous sulfate (10 µg/ml) as controls for free iron ion-induced neurotoxicity.

In order to determine protein expression using Western Blot analysis, cells were washed with cold Tris-buffered saline (TBS) and harvested in immunoprecipitation buffer (RIPA buffer with 1 % cOmplete Ultra Mini EDTA-free protease inhibitor cocktail, 1 % protease inhibitor cocktails 2 and 3, and 1 mM phenylmethanesulfonyl fluoride (PMSF). The lysates were then rotated at 4 °C for 30 min, followed by centrifugation at 14,000×g for 20 min. The supernatants were used for Western blot analysis of proteins where a fixed amount of protein

was resolved on SDS-PAGE gels and subjected to immunoblot analyses using antibodies for c-Abl, Phospho-c-Abl, and alpha-synuclein. Immunoblot signals were visualized using enhanced chemiluminescence reagent (Pierce, USA). Methamphetamine (METH; 500 μ M) served as the positive control. In some cases, cells were analyzed for dopamine content using HPLC with electrochemical detection [18].

Cellular proliferation was assessed using a 5-Bromo-2'-deoxy-uridine (BrdU) Cell Proliferation-labeling and detection kit III (Roche) following the manufacturer's instructions. Briefly, BrdU was added to cells and incubated for specified exposure durations with the compound(s) of interest. BrdU containing media was then removed and the cells fixed (ethanol 70 %, hydrochloric acid 25 %, H₂O 5 % for 30 min at -20 °C). Nucleases were added for 30 min (37 °C) to digest the BrdU-labeled DNA. Samples were then incubated for 30 min (37 °C) with anti-BrdU-peroxidase (POD). POD substrate was added and the absorbance measured using a SynergyMX plate reader (BioTek) after 15 min at 405 nm with a reference wavelength of 490 nm. Ferric chloride (FeCl₃) and ferric sulfate (Fe₂(SO₄)₃) at 10 μ g/mL served as positive controls. METH (500 μ M) served as the negative control.

To assess changes in mitochondrial function, cells were grown in half volume 96 well-plates (Greiner-Bio One, Monroe, NC) and treated with compound(s) of interest. After specified exposure periods, treatment media were removed and live cells were stained at 50 μ L per well with a combination of 2.5 μ g/mL Hoechst 3342 (Invitrogen, City, State) and 100 nm MitoTracker[®] Orange CMTMRos (Invitrogen) for 30 min. FeCl₃ and Fe₂(SO₄)₃ (10 μ g/mL) served as positive controls. METH (500 μ M) served as the negative control. Subsequent imaging of the cells is described below.

Assessing activation of caspases 3 and 7 was accomplished using methods identical to the process described above with 7.5 μ M CellEvent Caspase 3/7 Green Detection Reagent[®] (Invitrogen) substituted for MitoTracker. For Caspase 3/7 assays, Fe₂(SO₄)₃ (10 μ g/mL), cadmium (50 μ M), and thimerosal (100 μ M) served as positive controls. METH (500 μ M) served as the negative control. For both MitoTracker and Caspase 3/7 assays, six sites per well were imaged at 20 \times using an ImageXpress XL (Molecular Devices, Sunnyvale, CA) outfitted with DAPI and CY3 filters. DAPI and CY3 exposures for MitoTracker were 10 and 20 ms, respectively. Exposures for Caspases 3/7 were 10 and 100 ms, respectively. Images were subsequently analyzed using the MetaXpress Multiwavelength Cell Scoring Module (Molecular Devices). The module quantified the percent of cells (identified by Hoechst stain) positive for either the MitoTracker or Caspase 3/7 stains. Data were then statistically analyzed using AcuityXpress (Molecular Devices) and SigmaStat.

The reactive oxygen species (ROS) assay was performed using 2', 7'- di-chlorofluorescein di-acetate (DCFH-DA), a non-ionic, non-polar compound that crosses cell membranes

and is hydrolyzed enzymatically by intracellular esterases to non-fluorescent DCFH. DCFH is oxidized by ROS to highly fluorescent dichlorofluorescein (DCF). As a result, intracellular DCF fluorescence can be used as a metric with which to quantify the overall oxidative stress in cells [19]. Briefly, DCFH-DA (200 μ M, final concentration at 100 μ L per well) in assay media was added to all wells of a 96-well plate. Subsequently, nanoparticles (final concentration of 2.5, 5, or 10 μ g/mL) were added to each well and fluorescence measured 24 h later with a SynergyMX plate reader (excitation 485 nm, emission 530 nm). ROS was performed on SHSY-5Y cells and rat brain microvessel endothelial cells (rBMVEC). Data were expressed as percent of control levels of fluorescence. Ferric chloride (FeCl₃, 10 μ g/mL) was used as a positive control.

Blood–Brain Barrier Studies

Rat brain microvessel endothelial cells (rBMVEC) were isolated from rat brains as previously described [20]. All procedures with animals were carried out according to the National Institutes of Health Guide for the Care and Use of Laboratory Animals and approved by the NCTR/FDA Institutional Animal Care and Use Committee. Briefly, the meninges were mechanically removed and the gray matter was collected and minced through a 100- μ m-mesh screen. The enzyme Dispase II was added to the brain tissue for 1 h at 37 °C. The tissue was then centrifuged in a solution of 13 % dextran to separate the crude capillary vessels, which were collected and re-suspended in a collagenase/dispase enzyme solution and incubated for 1.3 h at 37 °C. The digested capillaries were centrifuged to remove the enzymes and then placed into percoll gradient tubes and centrifuged to separate the rBMVECs, which were extracted from the percoll gradient and seeded onto collagen-coated, fibronectin-treated plates in MEM-F12 media with 20 % FBS and then placed into a humidified incubator (37 °C, 5 % CO₂) until confluent (typically 12–14 days).

Permeability assays were performed to investigate monolayer integrity by measuring fluorescein flux as previously described [21]. Upon attaining confluence, cells seeded on 24 mm, 0.4- μ m pore size, polycarbonate membrane inserts (Costar) were exposed to Fe-NPs on their apical (intravascular side). After 24 h of treatment, polycarbonate membrane inserts were removed with a scalpel and transferred to permeability chambers (Permeagear, Hellertown, PA) that were attached to a water circulator set at 37 °C. Assay buffer II (sodium chloride 122 mM, potassium chloride 3 mM, calcium chloride 1.4 mM, magnesium sulfate 1.2 mM, sodium bicarbonate 25 mM, HEPES 10 mM, glucose 10 mM, K₂HPO₄ 0.4 mM, pH 7.4) was placed on both apical and basolateral sides (2 mL each side) with 10- μ m fluorescein added to the apical side. For the first hour, assay buffer II on the basolateral side was removed every 15 min (T0, T15, T30, T45, and T60) and replaced with 2 mL of fresh buffer. During the second hour, this was done

every 30 min (T90 and T120). At the end of 2 h, samples (200 μ L) from removed basolateral buffer were plated in triplicate and fluorescein concentration determined using a SynergyMX plate reader (BioTek, Winooski, VT) with an excitation wavelength of 485 nm and an emission wavelength of 530 nm. Data (in relative fluorescent units, rfu) were expressed as sum concentration of fluorescein flux over 120 min.

Trans-endothelial electrical resistance (TEER) readings were taken with an epithelial volttohmmeter (EVOM2, World Precision Instruments, Sarasota, FL) as an index of tight junction closure. Completely, confluent monolayers of rBMVECs used for these experiments were seeded in 0.4- μ M pore size trans-wells. TEER readings were taken after 24 h Fe-NPs exposure. Confluence was designated by TEER reading of 180 Ω [22]. The resistance of a coated trans-well without the cells was subtracted from the readings.

Animal Studies

Adult male wild-type Sprague Dawley rats ($n=10$ per group) were used in these studies. Animals were obtained from the vivarium at NCTR/FDA. All procedures were carried out in strict accordance with the National Institutes of Health Guide for the Care and Use of Laboratory Animals and the NCTR/FDA Institutional Animal Care and Use Committee. Rats were injected i.v., either with saline or a saline suspension of Fe-NPs (50 mg/kg b. wt., 1 h before beginning of the MRI scans).

Rats from each group were humanely sacrificed by decapitation using a small animal decapitator (Harvard Instruments, city, state) 72 h after Fe-NP injection. The striata were dissected on ice, flash-frozen, and stored at -80 $^{\circ}$ C until further analysis. In some cases, rats were anesthetized with sodium pentobarbital, perfused, and brain tissue was excised and fixed in 2 % paraformaldehyde.

For magnetic resonance imaging and spectroscopy (MRI/S) studies, rats were repeatedly scanned using magnetic resonance imaging and spectroscopy 1 h after treatment with Fe-NPs or saline. MRI/S was performed using a Bruker BioSpec 7T/30 system with a bird-cage transmit and a four-channel phased array receive coil. Animals were anesthetized using isoflurane general anesthesia (3 % induction, 1–2 % maintenance in 1 L/min oxygen) and the body temperature maintained at 37.0 ± 0.5 $^{\circ}$ C for the duration of scans. MRI/S protocol consisted of dynamic T_1 -weighted imaging (detection of iron dynamics), T_2 mapping (detection of iron-induced relaxation changes), and spectroscopy. Dynamic imaging was performed using gradient echo sequence (TE=2.65 ms, TR=208 ms, FOV=3.84 \times 3.84 cm, matrix 384 \times 288 \times 1, 1 min/image, 60 images train). Whole brain T_2 relaxation mapping was performed using a multi-echo, spin echo sequence (FOV=3.84 \times 3.84 \times 2.4 cm, matrix 192 \times 192 \times 24, 16 echoes with 15 ms spacing, TR=6 s, NA=1). MRI T_2 maps were produced from original multi-echo images using pixel-by-pixel simple

exponential fitting. Brain tissue images without surrounding tissues and ventricles were extracted from resultant T_2 maps and averaged across the animals. Statistical analysis of T_2 changes was performed using paired t test. MR spectra were acquired from striatum using PRESS sequence with VAPOR water suppression and outer volume saturation with the following parameters: TE=8.0 ms, TR=2.5 s, NA=256. Reference spectra (without water suppression) from the same regions were acquired for eddy current corrections and water scaling using LCMoDel software. Statistical analysis of MRS data was performed using repeated measures ANOVA.

The concentrations of catecholamines (dopamine, 3,4-dihydroxyphenylacetic acid and homovanillic acid) were determined in striatal tissues using a modified HPLC method combined with electrochemical detection. Tissues were weighed in a measured volume (20 % w/v) of 0.2 M perchloric acid containing the internal standard 3,4-dihydroxybenzylamine (100 ng/ml). The tissues were disrupted by ultrasonication and centrifuged at 4 $^{\circ}$ C (15,000 \times g; 7 min), and 150 μ l of the supernatant was removed and filtered through a Nylon-66 microfilter (pore size 0.2 μ m; MF-1 centrifugal filter; Bioanalytical Systems, city, state). Aliquots of 25 μ l representing 2.5 mg of brain tissue were injected directly onto the HPLC/ECD system for separation of analytes. The concentrations of catecholamines were calculated using a standard curve that was generated by determining in triplicate the ratio between three different known amounts of the amine and a constant amount of internal standard [18].

For immunostaining [23], the localization of tyrosine hydroxylase (TH), dopamine transporter (DAT), and rat epithelial cell antigen (RECA-1) was assessed in coronal slides (20 μ m) permeabilized with 0.1 % Triton X-100 for 10 min. Non-specific immunostaining was prevented by blocking for 30 min with 10 % goat or horse serum at room temperature. Sections were incubated for 2 h with rabbit anti-TH (1:2000, Millipore), mouse-anti-DAT (1:1000, Sigma), and mouse anti-RECA antibodies (1:500, Sigma) overnight, followed by biotin-anti-rabbit or mouse IgG (1:2000). After that, avidin:biotin conjugated HRP was added for 1 h. Finally, diaminobenzidine was added in order to develop the dark-brown color, and the tissue was mounted and clarified with xylene. Photomicrographs were taken using a light microscope (Nikon eclipse Ni, NIS-elements 4.2 software). Qualitative analysis of the staining was performed in the striatum and substantia nigra ($n=3$). Future quantitative analysis was performed by Western blot.

Results

Physical and Chemical Characterization of Fe-NPs

The Fe-NPs used in this study as reported by the manufacturer (Ocean Nanotechnology Inc., AR) had a core size of 10 and

30 nm with a diameter of 8–10-nm surface coating. The size, size distribution, surface charge, and shape of the Fe-NPs were evaluated and validated using TEM and Zetasizer. Using transmission electron microscope (TEM), the primary size of the 10 and 30 nm Fe-NPs was determined to be 10.8 ± 0.2 and 30.1 ± 1.8 nm (mean \pm SD), respectively (Table 1). The TEM images (Fig. 1a) obtained show the spherical shape and uniform size distribution of the materials used in this study. EDS analysis (Fig. 1b) confirmed the presence of the elements Fe in the sample. The large C and Cu peaks are due to the Cu grid and the grid coating of carbon materials. The chromium (Cr) peak was from the internal column of the TEM microscope. The oxygen (O) peak is from the sample or working environment. Zetasizer analysis based on dynamic light scattering (DLS) indicated that the average size of 10 and 30 nm Fe-NPs in water solution were 23.2 ± 0.2 and 39.8 ± 0.5 nm (mean \pm SD). The average zeta potential of 10 and 30 nm Fe-NPs in water solution were -33.9 ± 2.3 and -32.9 ± 0.4 mV, respectively (Table 1), suggested the testing Fe-NPs with the negative charge in their surfaces. The average polydispersity index of 10 and 30 nm Fe-NPs in water solution were 0.13 ± 0.01 and 0.08 ± 0.01 mV, respectively (Table 1), indicating the monodisperse nanoparticle solution used in this study. TEM directly measured the core size of the nanoparticles based on the projected area, while DLS measured the hydrodynamic size of the nanoparticles based on the hydrodynamic diffusion area of the particle being measured. The hydrodynamic diameter by DLS is about 10–12 nm larger than the TEM determined diameter by an offset that is a function of surface capping agent. Therefore, DLS provides the additional information compared with size measured by TEM.

Fe-NPs Deplete Dopamine and Activate Cellular Death Pathway in Dopaminergic Neuronal Cell Cultures

To understand the primary neurotoxic effects of Fe-NPs, SHSY-5Y human neuroblastoma cells (SHSY-5Y cells) were exposed to 10 μ g/ml of 10 and 30 nm Fe-NPs. After a 24-h exposure to 10 and 30 nm nanoparticles, cellular dopamine content was depleted by 68 and 52 %, respectively (Fig. 2a). In addition, exposure to Fe-NPs also resulted in activation of c-Abl, a molecular switch induced by oxidative stress, as evidenced by phosphorylated c-Abl tyrosine kinase (pY245-c-Abl), and increased expression of neuronal α -synuclein, a protein marker for toxic neuronal injuries (55 and 38 %, respectively; Fig. 2b). These data suggest that the exposure to Fe-NPs leads to a depletion of dopamine in neuronal cells that results in activation of oxidative stress pathways yielding dopaminergic neurotoxicity via protein dysfunction.

Table 1 Summary of characterization of 10 and 30 nm Fe-NPs

Physical Parameters	Fe-NPs-10 ^a	Fe-NPs-30 ^a
Primary size (nm)	10.8 \pm 0.2	30.1 \pm 1.8
Hydrodynamic size (nm)	23.2 \pm 0.2	39.8 \pm 0.5
Shape	Spherical	Spherical
Polydispersity Index	0.13 \pm 0.01	0.08 \pm 0.01
Zeta potential ζ (mV)	-33.9 \pm 2.3	-32.9 \pm 0.4

^a 10 nm of Fe-NPs (Fe-NPs-10) and 30 nm of Fe-NPs (Fe-NPs-30) were dispersed in water solution and sonicated for 5 min. Dilution of Fe-NPs was transferred to a cuvette or Zeta Potential cell for dynamic size or zeta potential measurement. The primary size and shape of the nanoparticles were determined by TEM

Fe-NPs Inhibit Cellular Proliferation, Alter Mitochondrial Integrity, and Activate Pro-apoptotic Caspases

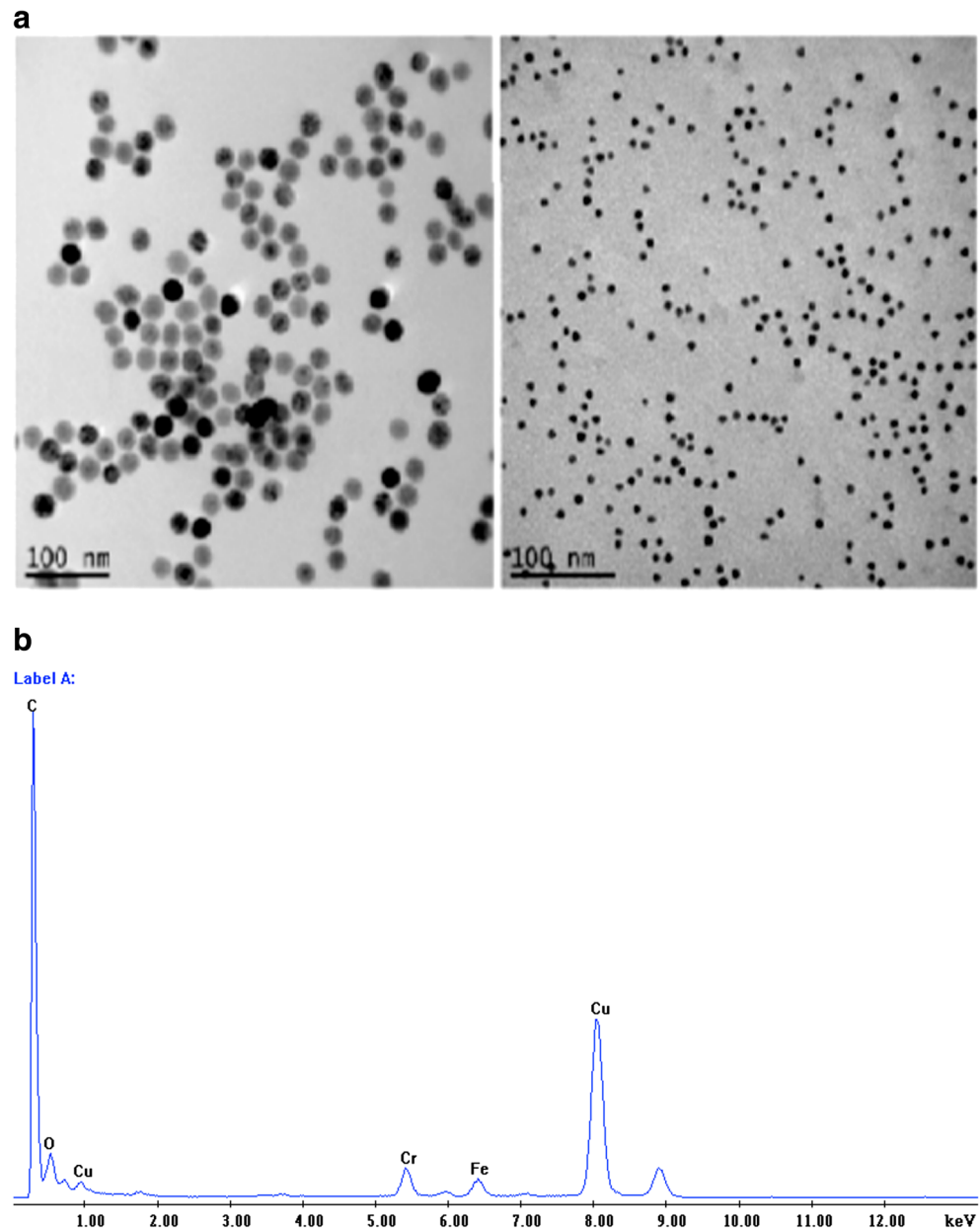
To further understand the mechanism of Fe-NP-induced dopaminergic neurotoxicity, we performed analysis of cell proliferation in SHSY-5Y cells exposed to 10 and 30 nm Fe-NPs (2.5, 5, or 10 μ g/ml). Among all the doses studied, only the 10 μ g/ml dose of 10 nm Fe-NPs significantly reduced cell-proliferation after 24 h as assayed using BrdU-incorporation into newly dividing cells (Fig. 2c).

To clarify the role reactive oxygen species (ROS) play in Fe-NPs toxicity, ROS assay was performed in SHSY-5Y cells exposed to 10 and 30 nm Fe-NPs (2.5, 5, or 10 μ g/ml). A dose-dependent increase in ROS was observed for both 10 and 30 nm Fe-NPs, with significant increase relative to control visible at 2.5 and 5 μ g/mL, respectively (Fig. 2d). For 10 nm Fe-NPs, all doses were statistically different. For 30 nm Fe-NPs, 5 and 10 μ g/mL were statistically different.

To further relate the induction of oxidative-stress pathway to the resulting neurotoxicity of Fe-NPs, we performed high-throughput MitoTracker imaging analysis of SHSY-5Y cells exposed to 10 or 30 nm Fe-NPs (2.5, 5, 10, 20, or 40 μ g/ml). A significant reduction in the number of active mitochondria was observed in neuronal cells 24 h after exposure to 20–40 μ g/mL of 10 or 30 nm Fe-NPs, suggesting an increase in reactive oxygen species (ROS) (Fig. 2e). Images (Fig. 2f) of mitochondria that were stained green in live cells (nuclei stained blue with DAPI) suggested that Fe-NPs affected mitochondrial integrity. This finding and the observation that ferric chloride or ferrous sulfate resulted in a high degree of inhibition of cellular proliferation (Fig. 2c) suggest that the cells are undergoing apoptotic rather than necrotic death, as indicated by nuclear symmetry in cells exposed to ferric chloride. Necrotic nuclei would appear highly fragmented without any pattern characteristic of nuclei. The possible apoptotic mechanism(s) induced require further elucidation.

In order to assess whether the neurotoxic effects of Fe-NPs on SHSY-5Y dopaminergic neurons are mediated by

Fig. 1 a Characterization of Fe-NPs using transmission electron microscopy (TEM). The *left panel* shows 80,000 \times TEM image of 30 nm Fe-NPs. The *right panel* shows 80,000 \times TEM image of 10 nm Fe-NPs. Fe-NPs display spherical morphology and uniform size distribution. **b** Elemental distribution of samples as determined by energy dispersive spectroscopy (EDS). EDS confirmed the presence of the elements Fe, carbon (C), and Copper (Cu) and indicated a high purity of the iron nanomaterials. The large C and Cu peaks are due to the Cu grid and the grid coating of carbon materials. The chromium (Cr) peak was from the internal column of the TEM microscope. The oxygen (O) peak is from the working environment/sample holder background



apoptosis, high-throughput caspase 3/7 activation analyses were performed after exposure to 2.5–40 $\mu\text{g}/\text{ml}$ of 10 or 30 nm Fe-NPs (Fig. 2g). Neuronal cells were exposed to cadmium (50 μM), ferrous sulfate (10 $\mu\text{g}/\text{mL}$), and thimerosal (100 μM) as positive controls; METH (500 μM) was used as the negative control. Caspase 3/7 imaging of $\frac{1}{2}$ volume 96-well plates occurred with six images obtained for each well; each image represented a single data point. Imaging was performed in a MetaXpress IXM XL instrument (Molecular Devices). Data were further analyzed in Acuity Xpress (Molecular Devices). Three optimal clusters were determined (supplemental 1) and data displayed in a principal component analysis (PCA) plot utilizing percent of caspase positive cells, mean area of all

cells, mean area of all nuclei, and mean caspase-positive stain intensity for each data point (Fig. 2g). Here, 854 data points fall into the “green” cluster, 521 data points into the “red” cluster, and 284 data points into the “yellow” cluster (supplemental 1). All doses of 10 and 30 nm Fe-NPs and control treatments are found in the “green” cluster. The “red” cluster also contains all doses of 10 and 30 nm Fe-NPs, and control treatments, but also contains the negative control group methamphetamine. Note that the cluster difference between the “red” and “green” group is likely the result of a plate effect, not a treatment effect (i.e., data points from red cluster were all from the same plate; green cluster data were from the same plate, run on a different day). Notably, the “yellow” cluster contains only 10 nm Fe-NPs at

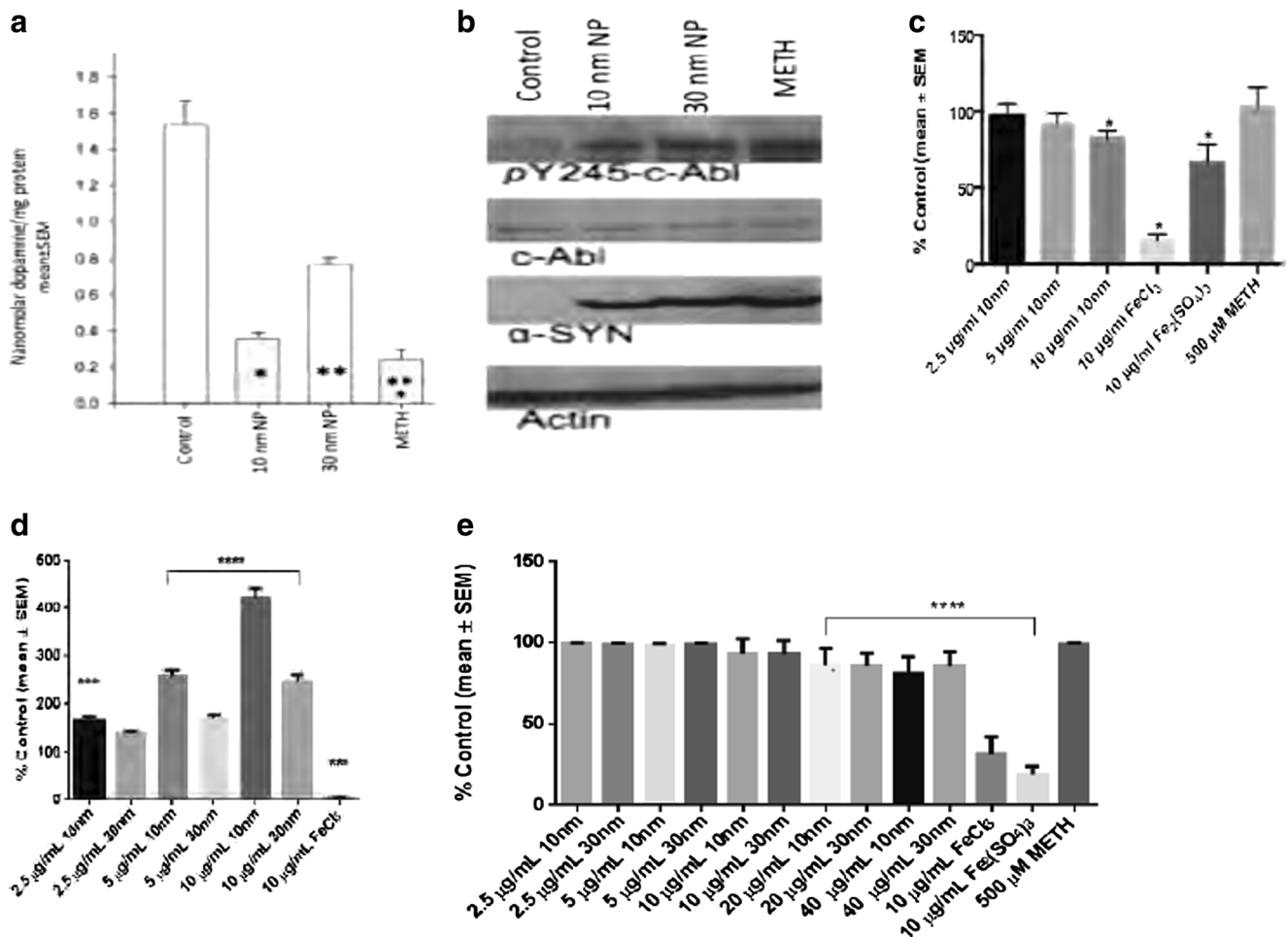


Fig. 2 **a** Dopamine levels were measured utilizing HPLC-ECD. Dopamine levels in SHSY-5Y cells treated with 10 or 30 nm Fe-NPs (10 µg/ml) or METH (500 µM) for 24 h in low serum medium. * $p < 0.05$ significant versus control; ** $p < 0.05$ significant versus control and 10 nm Fe-NPs; *** $p < 0.05$ significant versus control, 10 and 30 nm Fe-NPs. Differences among means were analyzed using one-way analysis of variance (ANOVA) followed by Newman-Keuls post hoc analysis. **b** Representative immunoblots of SHSY-5Y cell lysates treated with 10 or 30 nm Fe-NPs (10 µg/ml) or METH (500 µM) for 24 h in low serum medium. Blots were incubated with phospho-c-Abl (pY245-c-Abl on the figure), c-Abl, alpha-synuclein, and actin antibodies. **c** Cell proliferation in SHSY-5Y cells exposed to 10 and 30 nm Fe-NPs (2.5, 5, or 10 µg/ml) for 24 h determined by BrdU assay. At 10 µg/ml dose of 10 nm, Fe-NPs significantly reduced cell-proliferation. * $p < 0.05$ = significantly different versus control. Differences among means were analyzed using one-way analysis of variance (ANOVA) with the different treatments as the independent factor followed by Newman-Keuls post hoc analysis. **d** Reactive oxygen species (ROS) in SHSY-5Y cells treated with 10 or 30 nm Fe-NPs (2.5–10 µg/mL). FeCl₃ (10 µg/mL) served as the positive control. *** $p < 0.001$ significant versus control, **** $p < 0.0001$ significant versus control. Differences among means were analyzed using one-way analysis of variance (ANOVA) followed by Tukey's post hoc analysis. **e** Active mitochondria as percent of control in SHSY-5Y cells

treated with 10 or 30 nm Fe-NPs (2.5, 5, 10, 20, or 40 µg/ml). FeCl₃ (10 µg/mL) and Fe₂(SO₄)₃ (10 µg/mL) served as positive controls. METH (500 µM) served as a negative control. Treatments were for 24 h in low serum medium. Active mitochondria were imaged using an IXM XL unit at 20× and the data quantified using the multi-wavelength cell-scoring module in MetaXpress. **** $p < 0.0001$ significant versus control. Differences among means were analyzed using one-way analysis of variance (ANOVA) followed by Sidak's post hoc analysis. **f** Representative images from MitoTracker analysis at 20× where green represents live cells and blue represents DAPI staining of nuclei in SHSY-5Y cells. All experiments were repeated at least three times and representative examples are presented. **g** Principle component analysis of high content imaging of caspase 3/7 stain in SHSY-5Y cells exposed to 10 or 30 nm Fe-NPs in concentrations ranging from 2.5 to 40 µg/ml. Here, the negative control was METH (500 µM) and positive controls were thimerosal (100 µM), cadmium (50 µM), and ferrous sulfate (10 µg/mL). Three clusters (red, yellow, and green) were identified as important components as indicated by self-organizing maps (SOM) and GAP statistics (see supplementary materials). Note the cluster difference between the red and green group likely arose from a plate effect, not a treatment effect. For all figures, values are expressed as mean values per group ± SEMs

10–40 µg/mL and the positive controls cadmium, ferrous sulfate, and thimerosal. These PCA data suggested that only 10 nm Fe-NPs increases caspase 3/7 activation, thereby

contributing to apoptosis. These data also suggested that bigger size nanoparticles might not produce significant neurotoxicity, especially via apoptosis.

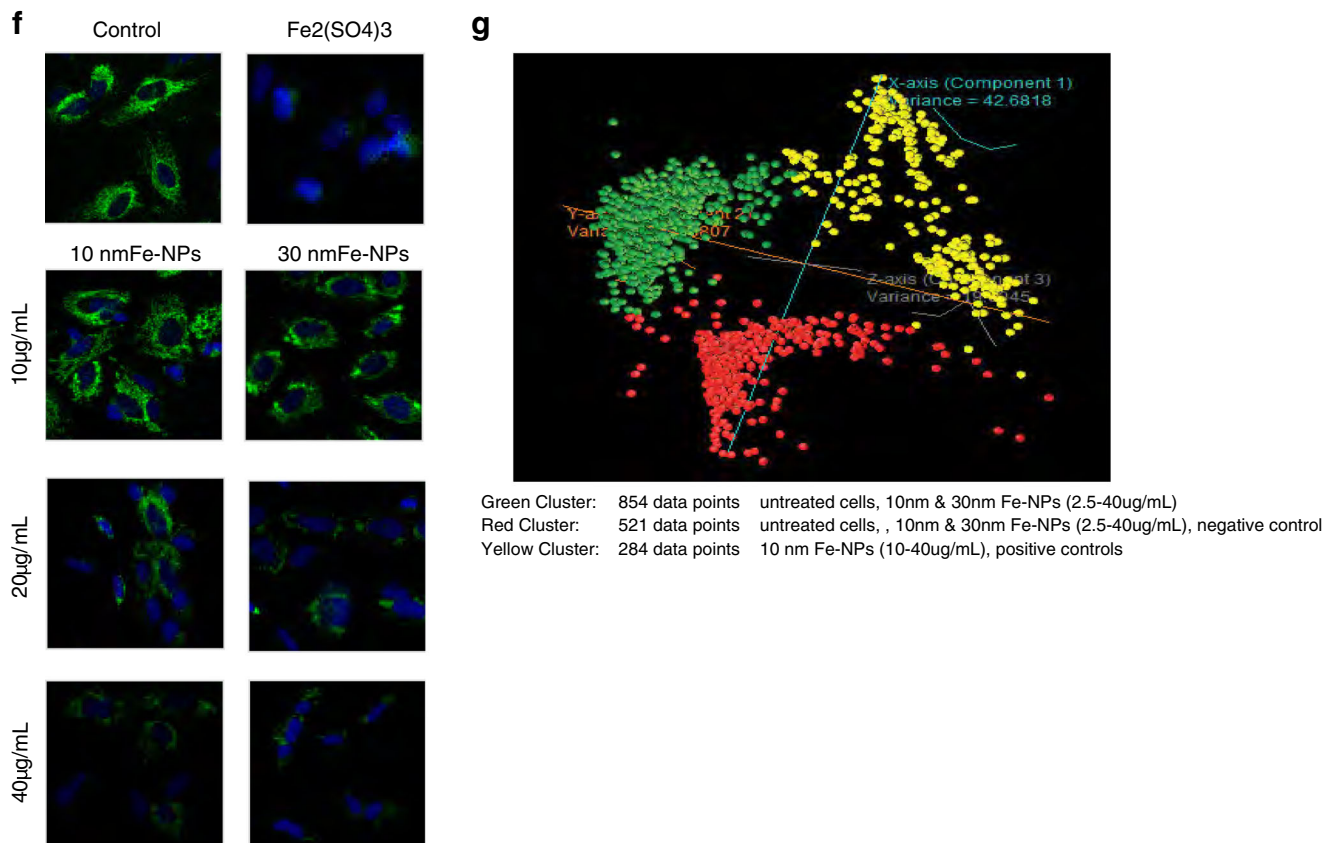


Fig. 2 (continued)

Fe-NP-Induced Neurotoxicity Might Result from a Compromised Blood–Brain Barrier

To further evaluate the impact of Fe-NPs-induced neurotoxicity, we investigated whether Fe-NPs exposure would alter the integrity of the blood–brain-barrier (BBB). Artificial BBBs comprised of rBMVECs were exposed to 10 μg/ml of 10 and 30 nm Fe-NPs for 24 h and demonstrated that Fe-NPs significantly increased fluorescein efflux across the rBMVECs over 120 min post-exposure (Fig. 3a). Although no significant difference was observed between the degrees of efflux caused by 10 and 30 nm Fe-NPs, a slightly larger effect of 10 nm Fe-NPs was seen in the TEER permeability measure (Fig. 3b). Therefore, to further understand the mechanism(s) by which Fe-NPs might compromise BBB integrity, production of reactive oxygen species (ROS) was assessed after exposure to increasing concentrations of 10 nm Fe-NPs. A highly significant dose-dependent increase in ROS was observed 24 h after the exposure of rBMVECs to 10 nm Fe-NPs as compared to non-treated controls (Fig. 3c). These data suggested that the neurotoxic effects of Fe-NPs might be mediated by their potential to damage the BBB. Based upon these findings, the effects of Fe-NPs exposure in vivo were investigated.

Fe-NP Exposure Induces Brain Water Relaxation Changes and Neurochemical Alterations in Rat Striatum

MRI was utilized to probe T₂ changes in living brain following exposure of rats to a single dose (50 mg/kg b.wt.) of 10 nm Fe-NPs. This approach was based on the assumption that Fe-NPs change water relaxation, both T₁ and T₂, which could thus be used as a measure of Fe-NP brain penetration. A significant decrease in T₂ signal was observed after a single injection (Fig. 4a). A typical example of the T₂ changes detected in adult rats after 10 nm Fe-NP administration is shown in Fig. 4b. It can be seen that Fe-NP treatment induced noticeable decreases in brain T₂ images that are suggestive of Fe-NPs penetration into the brain. Additionally, dynamic T₁-weighted observations after injection of 10 nm Fe-NP confirmed the transfer and retention of these particles from brain vasculature to brain tissue (Fig. 4c; Supplementary video 1).

Furthermore, in vivo MRS suggested local changes in the neurochemical environment of the striatum after the exposure to a single dose of 10 nm Fe-NP. All metabolites observed during spectroscopy were expressed in their absolute concentrations, based on the intrinsic signal of the water from the same caudate-putamen or striatum voxel (Table 2).

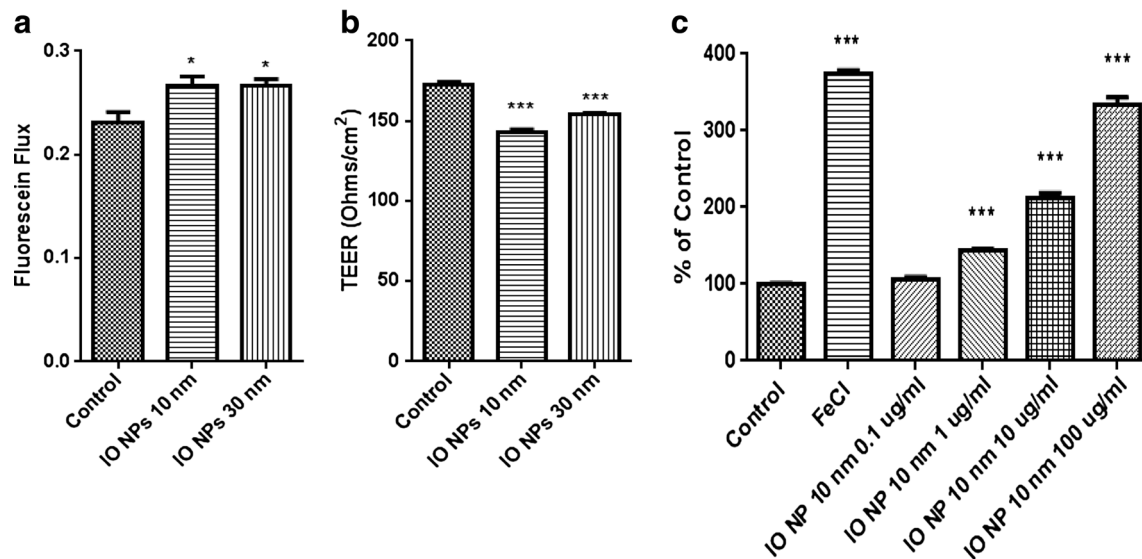


Fig. 3 The sum of fluorescein efflux (a) over 120 min was determined using a plate reader at excitation 485 nm and emission 530 nm; results are expressed in relative fluorescent units (rfu); $N=9$. Trans-endothelial electrical resistance (TEER) (b) was measured in rBMVECs 24 h after exposure to 10 $\mu\text{g/ml}$ of 10 and 30 nm Fe-NPs; $N=9$. Reactive oxygen species (c) were measured in rBMVECs 24 h after treatment with 10 nm

Fe-NPs (0.1–100 $\mu\text{g/ml}$). Ferric chloride (FeCl_3 , 10 $\mu\text{g/ml}$) served as the positive control. $N=3$ per data point. Differences among means were analyzed using one-way analysis of variance (ANOVA) followed by Newman-Keuls post hoc analysis. For all figures, values are expressed as mean values per group \pm SEMs. * $p<0.05$ and *** $p<0.001$ as compared to the control group

Fe-NP Exposure Induces Neurotoxic Changes in Dopaminergic Phenotype Followed by Dopamine Neuronal Loss

Because of the neurochemical alterations seen via MRS of the striatal region, we sought to also evaluate the effect of 10 nm Fe-NPs on the dopamine content in the striatum. Analyses of dopamine and its metabolites, DOPAC (3,4-dihydroxyphenylacetic acid) and HVA (homovanillic acid), in the striatum 72 h after a single injection of 50 mg/kg of 10 nm Fe-NPs revealed a significant decrease in their concentrations (Fig. 5a). These data provide direct evidence of dopaminergic neurotoxicity induced by an exposure to 10 nm Fe-NPs.

In order to further evaluate neuropathological correlate of dopaminergic neurotoxicity induced by 10 nm Fe-NPs, we performed immunohistopathological analysis of the striatum and substantia nigra pars compacta 72 h after rats were treated with a single dose (50 mg/kg) of 10 nm Fe-NPs. A significant decrease in dopamine transporter binding in both the striatum (Fig. 5b left panels) and the substantia nigra (Fig. 5b right panels) were observed. Additionally, treatment with 10 nm Fe-NPs significantly decreased the number of tyrosine hydroxylase positive neurons in the striatum (Fig. 5c left panels) and tyrosine hydroxylase positive nerve terminals in the substantia nigra (Fig. 5c right panels) of animals treated with the Fe-NPs. These data provide direct evidence of dopaminergic neurotoxicity followed by dopamine neuronal loss after exposure to 10 nm Fe-NPs. Finally, a significant decrease in the immunoreactivity of RECA-1, a rat endothelial cell antigen, was observed in the brains of animals treated with 10 nm

Fe-NPs (Fig. 5d). The reduction in RECA-1 is thought to represent damage to the brain vasculature after treatment with 10 nm Fe-NPs, which confirms the MRI imaging data showing reductions in T_2 -weighted relaxation after treatment with 10 nm Fe-NPs.

Discussion

With the increasing incorporation of engineered nanomaterials into almost every aspect of human health and lifestyle, one of the most important issues that must be addressed is the potential of these nanomaterials and their biodegradation products to cause toxicity [24–27]. Until now, the main mechanism thought to underlie the toxicity of nanomaterials has been related to their generation of oxidative stress via interaction with mitochondria [28]. Damage to the mitochondria by nanomaterials results in the leakage of electrons and increased oxidative stress [29]. Also, when administered systemically, nanomaterials have been shown to cross the blood–brain barrier (BBB) and access the CNS and induce edema [30].

Due to their superparamagnetic physicochemical properties, Fe-NPs have been found potentially applicable in the biomedical and industrial fields. Fe-NPs are commonly used for magnetic resonance brain imaging, serving as vectors for brain-targeted delivery of genes or drugs, and magnetic storage [1]. Due to the increasing application of Fe-NPs, studies evaluating their potential neurotoxicity have also grown in numbers. Studies performed using PC12 cells (rat pheochromocytoma cells that secrete catecholamines) have shown that

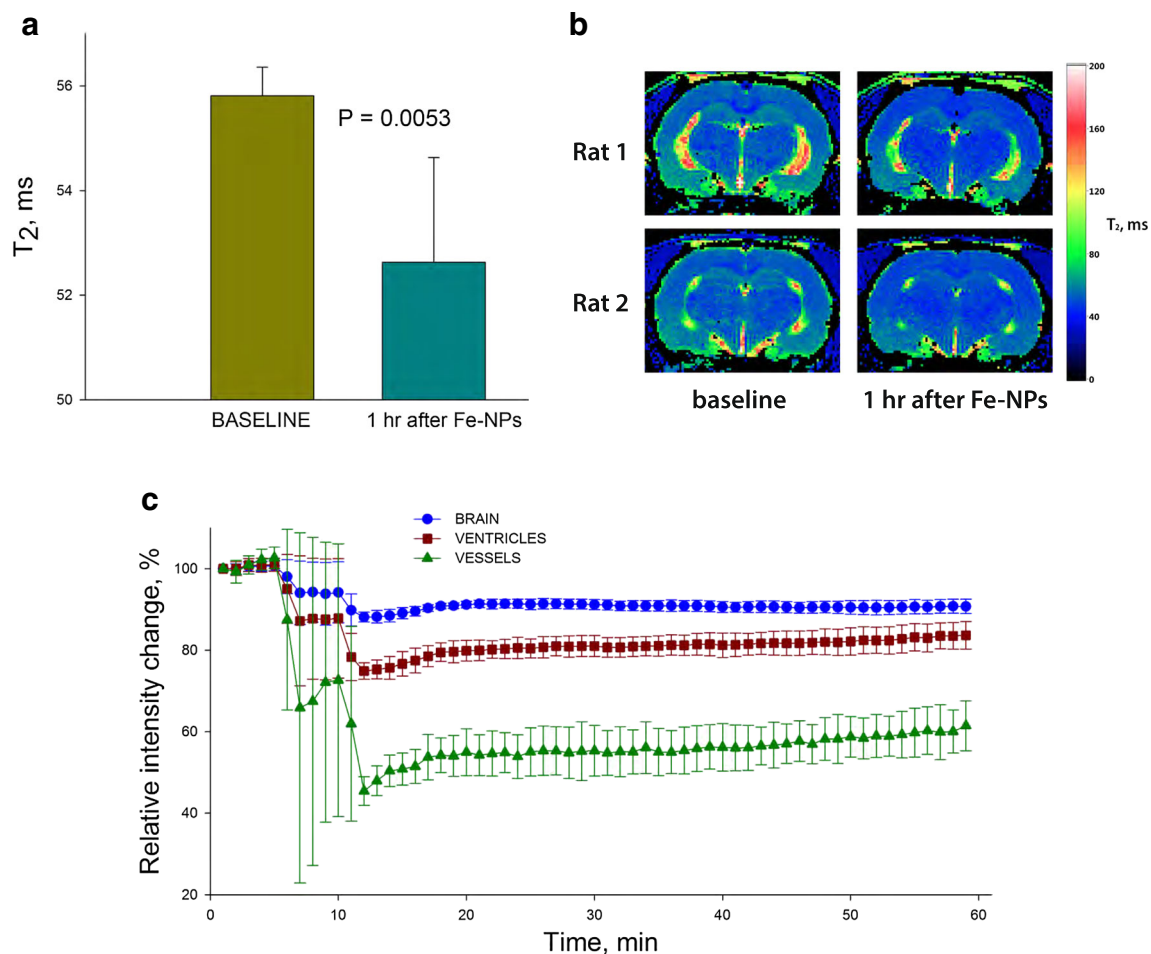


Fig. 4 Average MRI T_2 -weighted relaxation was reduced in rat brain 1 h after treatment with single dose (50 mg/kg) of 10 nm Fe-NPs. Representative T_2 maps (b) were produced from original multi-echo images using pixel-by-pixel simple exponential fitting. Brain tissue images were extracted from resultant T_2 maps, and histogram analysis was performed using procedures developed in-house using LabVIEW. Brain tissue was classified into three domains based on its T_2 value with arbitrary bands set at the following: 36–70 ms (normal intensity),

71–166 ms (high intensity), and 167–250 ms (cerebro-spinal fluid). The volume of the tissue falling into each band was quantified and averaged among groups. Statistical analysis was performed using one-way ANOVA on ranks with Dunn's post hoc multiple comparisons versus control using Sigma Plot software. A relative intensity scan (c) showed changes in relative intensity in large blood vessels, brain, and ventricles 1 h after a single injection of 10 nm Fe-NPs (50 mg/kg)

Fe-NPs can induce cytotoxicity [14]. Intranasal exposure to Fe-NPs led to their highest deposition in rat striata with a retention time of up to 14 days, thus, leading to an increase in oxidative stress in the striatum [15]. In the present studies, we sought to understand the mechanisms underlying Fe-NP induced damage to dopaminergic neurons utilizing human

neuroblastoma cells that mimic the phenotype of human dopamine neurons. It was observed that Fe-NPs, like the common dopaminergic toxicant methamphetamine (METH), caused dopamine depletion and increased α -synuclein expression. The fibrilization and aggregation of α -synuclein have been suggested to play a role in the development of

Table 2 MRS-detected neurometabolic changes in the striatum of rats after 50 mg/kg of 10 nm Fe-NP administration

Metabolite	Baseline	Time after Fe-NP injection 1 h	P (RM ANOVA) 72 h	
Glutamine	4.316 ± 0.402	4.375 ± 0.232	3.140 ± 0.083	0.001
Glutamate	12.655 ± 0.408	11.369 ± 0.442	11.556 ± 0.520	0.039
GSH	2.256 ± 0.139	2.574 ± 0.199	1.990 ± 0.045	0.043
Taurine	13.229 ± 0.571	11.727 ± 0.33	11.492 ± 0.350	0.050
Choline-containing compounds	2.430 ± 0.117	2.183 ± 0.117	2.256 ± 0.058	0.003

Data (mM) are mean ± SEM

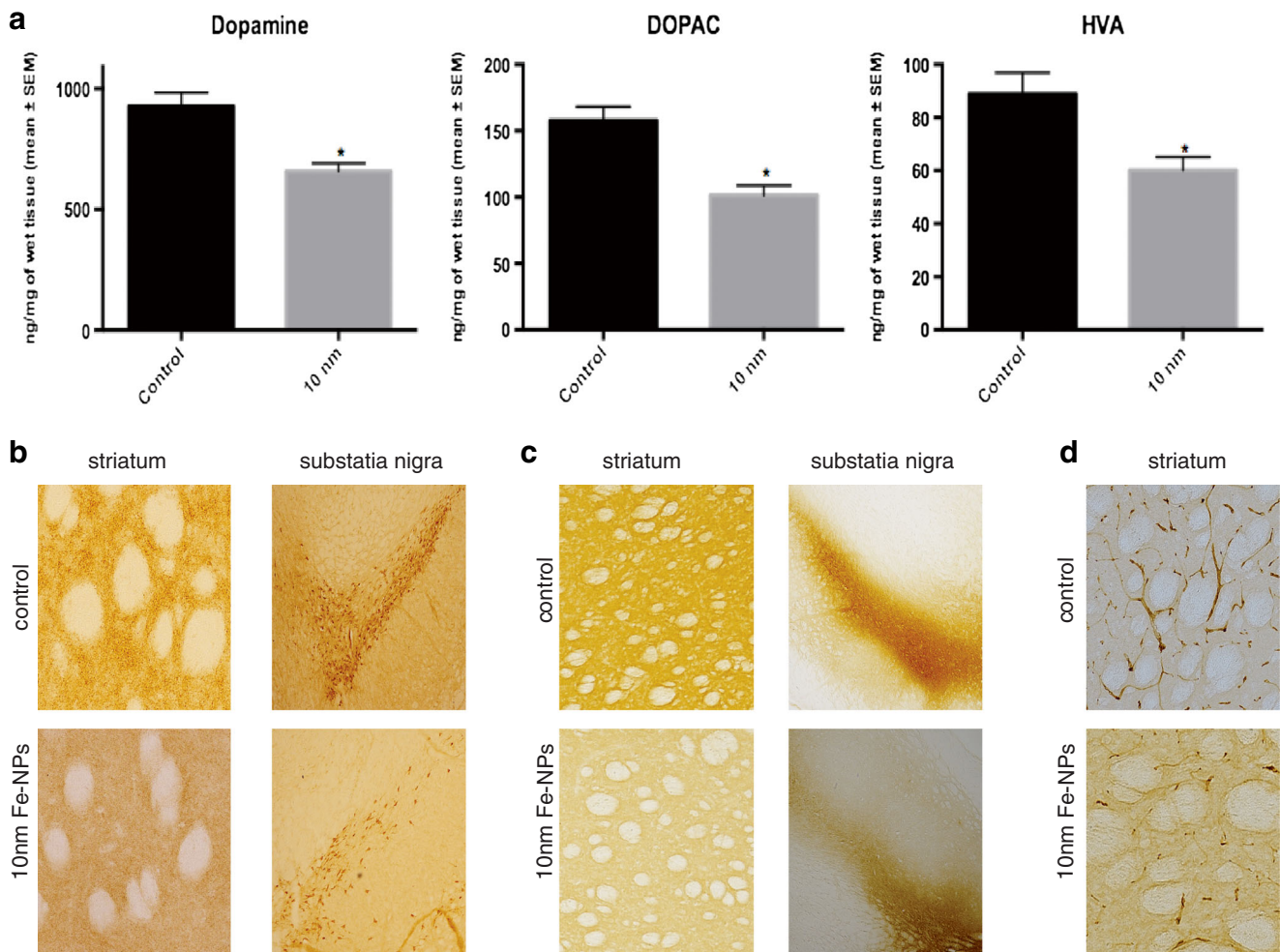


Fig. 5 **a** Levels of dopamine (DA) and its metabolites DOPAC and HVA were measured utilizing HPLC-ECD in the striatum of rats 72 h after treatment with a single dose (50 mg/kg b.wt.) of 10 nm Fe-NPs. $*p < 0.05$ = significantly different versus control. Differences among means were analyzed using one-way analysis of variance (ANOVA) with the different treatments as the independent factor followed by Newman-Keuls post hoc analysis; $N = 8$. Seventy-two hours after

treatment with a single dose (50 mg/kg) of 10 nm Fe-NPs, the striatum and substantia nigra of rat brains were immunohistochemically stained to investigate dopaminergic neuronal **(b)** loss of dopamine transporter (DAT) and **(c)** tyrosine hydroxylase (TH). **d** Visualization of brain vascular damage by immunohistochemical staining with rat endothelial cells antigen, RECA-1 in the striatum. Pictures were taken at $\times 10$ magnification

Alzheimer's and Parkinson's diseases [31]. The over-expression of α -synuclein and dopamine depletion observed in the present studies after Fe-NP treatment might have contributed to the increases in oxidative-stress that were indicated by the ROS assays. It has been recently demonstrated that oxidative stress activates a pro-death pathway in Parkinson's disease (PD) by the activation of a non-receptor tyrosine kinase c-Abl, leading to progressive death of dopamine neurons both in vitro and in vivo in animal models of PD [23, 18]. This oxidative stress mediated activation of c-Abl also seems to be associated with a neuronal death mechanism in human PD patients due to aggregation of toxic species of proteins [18]. In the present study, activation of c-Abl was observed after exposure to Fe-NPs. This activation of c-Abl, along with the increased expression of α -synuclein and loss of cellular dopamine, may lead to increased dopaminergic neuronal cell death

after exposure to Fe-NPs. It is interesting to note that Fe-NP exposure not only activated oxidative stress induced cellular death pathways in these dopaminergic neurons but also significantly reduced the cellular proliferation of these neuronal cells, as evidenced by reduced BrdU-incorporation, suggesting progressive neuronal damage.

To further understand the molecular pathways participating in dopaminergic neuronal death after exposure to Fe-NPs, the effect of Fe-NP exposure on mitochondrial integrity was evaluated in dopaminergic cells. Mitochondria serve as a major source of energy production and are responsible for maintaining the balance between cell survival and death [32, 33]. Mitochondrial dysfunction serves as an early sign of cellular damage [34], and the role of mitochondrial dysfunction in dopaminergic damage and neurological disorders is well known [35]. Recent studies have shown that Fe-NPs generate

loss of mitochondrial membrane potential [36] and cause genotoxicity via mitochondrial depolarization [37]. In the studies reported here, exposure to higher doses (20 and 40 $\mu\text{g/mL}$) of Fe-NPs led to a decrease in mitochondrial integrity, suggesting increased damage to mitochondrial membranes. Although Fe-NPs did significantly decrease mitochondrial integrity, neuronal cell loss was significantly higher with exposure to the ionic forms of iron. These observations suggested that Fe-NPs might induce an apoptotic cascade in these dopaminergic neurons via damage to mitochondrial membranes. The role of caspases as major players in inducing apoptosis is well known [38, 39]. Studies conducted in human breast cancer cells suggest that exposure to Fe-NPs leads to oxidative stress, DNA-damage, and caspase activation [40, 41]. Another study suggested there were increased levels of caspase mRNA and enzyme activity in skin and lung epithelial cells after exposure to Fe-NPs [42]. In the current studies, exposure to increasing concentrations of smaller size Fe-NPs led to a highly significant activation of caspases 3 and 7 in dopaminergic cells. Interestingly, only the smaller size Fe-NPs caused activation of caspases 3 and 7 in a fashion similar to that for prominent pro-apoptotic toxicants such as cadmium, thimerosal, and ferrous sulfate. This activation of caspases 3 and 7 in dopaminergic cells after exposure to Fe-NPs suggests that the neurotoxic damage caused by Fe-NPs is induced by oxidative stress that might be mediated via apoptotic mechanisms.

The *in vitro* data reported in the present study provides strong evidence that Fe-NPs produce neurotoxic damage to dopaminergic cells by activating an oxidative stress-mediated apoptotic cellular death pathway that leads to neuronal damage. In order for Fe-NPs to induce neurotoxic damage, it is imperative that they cross the BBB. A recent study suggested that a magnetic force-mediated mechanism serves to drag Fe-NPs through brain capillary endothelial cells in culture [43]. In the present studies, we sought to determine if Fe-NPs cross the BBB, and if they might also adversely affect the BBB. The data suggest that exposure to Fe-NPs results in an increased fluorescein efflux across cells in an *in vitro* model of the BBB comprised of rat brain microvessel endothelial cells (rBVMECs). Furthermore, exposure to Fe-NPs also resulted in an increase in trans-endothelial electrical resistance confirming damage to the model BBB. This was accompanied by an increased production of reactive oxygen species in the rBVMECs suggesting a role of oxidative stress in disturbing the integrity of the BBB model. Collectively, the present data suggest that exposure to Fe-NPs activates oxidative stress-mediated damage to dopaminergic cells that may result in a compromised BBB, thus, making the brain more vulnerable to subsequent Fe-NP exposure that might lead to more damage to dopaminergic neurons.

Taking into account the data presented here indicating that Fe-NPs are capable of disrupting the BBB, the effect of

exposure to Fe-NPs on the dopaminergic system in adult male rats was investigated. Magnetic resonance imaging followed by spectroscopy (MRI/S) was performed to evaluate the effects of a single exposure to 10 nm Fe-NPs. The MRI data contained evidence of Fe-NP transfer from blood to the brain ventricles, supporting the *in vitro* observation in the BBB model of compromised integrity after Fe-NP exposure. This transfer of Fe-NPs into brain ventricles was associated with a significant reduction in T_2 relaxation in the whole brain 1 h after exposure to single dose of 10 nm Fe-NPs. Furthermore, the associated anatomical changes observed in the striatum were followed by extensive neurochemical alterations as observed using MR spectroscopy. Previous MRS analyses—after a single exposure to 50 mg/kg of 10 nm Fe-NPs—showed that glutamate concentrations were significantly decreased reflecting altered neuronal activity [44]. Glutathione concentrations were also significantly increased 1 h after Fe-NP injection, suggesting a rapid compensation for increased ROS production; glutathione concentrations decreased 72 h after treatment, suggesting its depletion during ROS scavenging [45]. Taurine, which can be neuroprotective, was also significantly decreased, suggesting its consumption during cellular protection [46]. Choline-containing compounds, major membrane constituents, were also significantly decreased, likely the result of cellular membrane breakdown induced by lipid peroxidation [47].

Dopamine neurons are neuromelanin-rich cells that specifically express tyrosine hydroxylase (TH). This can be observed in cell bodies in the substantia nigra and in cell terminals in the striatum [48]. Additionally, high and specific expression of the dopamine transporter (DAT) serves as a functional marker [48]. A loss of TH-positive neurons reflects dopaminergic neuronal damage as evident in the most common animal models of PD [18]. A loss of DAT has been used as a biomarker for diagnostic purposes in various neurological disorders. The *in vivo* observations presented here of Fe-NP-induced anatomical and neurochemical changes, as observed via MRI and MRS, were further confirmed by loss of TH-positive terminals and DAT expression in the striatum as well as loss of TH-positive neurons and DAT expression in neurons in the substantia nigra. These data are unique observations of correlations between *in vivo* progressive brain anatomical and neurochemical changes after exposure to Fe-NPs and post-mortem neuropathology. Finally, a significant reduction in rat epithelial cell antigen-1 (RECA-1) was observed in the striatum following Fe-NP exposure. This reduction in RECA-1 (a marker of damaged brain vasculature) was also accompanied by significant morphological changes evident as shrinkage of neuronal vasculature in the striatum.

In summary, the present study is the first of its kind to show in real time the *in vivo* transfer of Fe-NPs from blood to brain and the impact of Fe-NPs on brain volume and chemistry.

Furthermore, the data show that oxidative stress and activation of the pro-death compound, c-Abl tyrosine kinase, are associated with Fe-NP induced neuronal damage and neurotoxicity. Furthermore, the data suggest protein dysfunction in neurons exposed to Fe-NPs via alterations in the expression of α -synuclein. These molecular pathways associated with neuronal damage have been implicated in various neurological disorders including Alzheimer and Parkinson's diseases. The anatomical, neurochemical and neuropathological changes observed in the present studies are common hallmarks of these devastating neurological disorders. The data suggest that smaller Fe-NPs may be able to directly access brain tissue by traversing the blood–brain barrier and cause neuronal damage to the dopaminergic system that is similar to that associated with these devastating neurodegenerative diseases.

Disclaimer The research reported here was funded by the NCTR/FDA protocol # E-07394.01. This document has been reviewed in accordance with US Food and Drug Administration (FDA) policy and approved for publication. Approval does not signify that the contents necessarily reflect the position or opinions of the FDA nor does mention of trade names or commercial products constitute endorsement or recommendation for use. The findings and conclusions in this report are those of the authors and do not necessarily represent the views of the FDA.

References

- Hood E (2004) Nanotechnology: looking as we leap. *Environ Health Perspect* 112(13):A740–749
- Wang B, Feng WY, Wang M, Shi JW, Zhang F, Ouyang H, Zhao YL, Chai ZF et al (2007) Transport of intranasally instilled fine Fe₂O₃ particles into the brain: micro-distribution, chemical states, and histopathological observation. *Biol Trace Elem Res* 118(3):233–243. doi:10.1007/s12011-007-0028-6
- Jain TK, Reddy MK, Morales MA, Leslie-Pelecky DL, Labhasetwar V (2008) Biodistribution, clearance, and biocompatibility of iron oxide magnetic nanoparticles in rats. *Mol Pharm* 5(2):316–327. doi:10.1021/mp7001285
- Mehta SH, Webb RC, Ergul A, Tawfik A, Dorrance AM (2004) Neuroprotection by tempol in a model of iron-induced oxidative stress in acute ischemic stroke. *Am J Physiol Regul Integr Comp Physiol* 286(2):R283–288. doi:10.1152/ajpregu.00446.2002
- Karmakar A, Zhang Q, Zhang Y (2014) Neurotoxicity of nanoscale materials. *J Food Drug Anal* 22(1):147–160. doi:10.1016/j.jfda.2014.01.012
- Simonian NA, Coyle JT (1996) Oxidative stress in neurodegenerative diseases. *Annu Rev Pharmacol Toxicol* 36:83–106. doi:10.1146/annurev.pa.36.040196.000503
- Imam SZ, Ali SF (2000) Selenium, an antioxidant, attenuates methamphetamine-induced dopaminergic toxicity and peroxynitrite generation. *Brain Res* 855(1):186–191
- Imam SZ, Islam F, Itzhak Y, Slikker W Jr, Ali SF (2000) Prevention of dopaminergic neurotoxicity by targeting nitric oxide and peroxynitrite: implications for the prevention of methamphetamine-induced neurotoxic damage. *Ann N Y Acad Sci* 914:157–171
- Imam SZ, Itzhak Y, Cadet JL, Islam F, Slikker W Jr, Ali SF (2001) Methamphetamine-induced alteration in striatal p53 and bcl-2 expressions in mice. *Brain Res Mol Brain Res* 91(1–2):174–178
- Imam SZ, Newport GD, Islam F, Slikker W Jr, Ali SF (1999) Selenium, an antioxidant, protects against methamphetamine-induced dopaminergic neurotoxicity. *Brain Res* 818(2):575–578
- Imam SZ, Newport GD, Itzhak Y, Cadet JL, Islam F, Slikker W Jr, Ali SF (2001) Peroxynitrite plays a role in methamphetamine-induced dopaminergic neurotoxicity: evidence from mice lacking neuronal nitric oxide synthase gene or overexpressing copper-zinc superoxide dismutase. *J Neurochem* 76(3):745–749
- Liberatore GT, Jackson-Lewis V, Vukosavic S, Mandir AS, Vila M, McAuliffe WG, Dawson VL, Dawson TM et al (1999) Inducible nitric oxide synthase stimulates dopaminergic neurodegeneration in the MPTP model of Parkinson disease. *Nat Med* 5(12):1403–1409. doi:10.1038/70978
- Binienda ZK, Beaudoin MA, Gough B, Ali SF, Virmani A (2010) Assessment of 3-nitropropionic acid-evoked peripheral neuropathy in rats: neuroprotective effects of acetyl-L-carnitine and resveratrol. *Neurosci Lett* 480(2):117–121. doi:10.1016/j.neulet.2010.06.020
- Pisanic TR 2nd, Blackwell JD, Shubayev VI, Finones RR, Jin S (2007) Nanotoxicity of iron oxide nanoparticle internalization in growing neurons. *Biomaterials* 28(16):2572–2581. doi:10.1016/j.biomaterials.2007.01.043
- Wu J, Ding T, Sun J (2013) Neurotoxic potential of iron oxide nanoparticles in the rat brain striatum and hippocampus. *Neurotoxicology* 34:243–253. doi:10.1016/j.neuro.2012.09.006
- Xue Y, Wu J, Sun J (2012) Four types of inorganic nanoparticles stimulate the inflammatory reaction in brain microglia and damage neurons in vitro. *Toxicol Lett* 214(2):91–98. doi:10.1016/j.toxlet.2012.08.009
- Zhang Y, Ferguson SA, Watanabe F, Jones Y, Xu Y, Biris AS, Hussain S, Ali SF (2013) Silver nanoparticles decrease body weight and locomotor activity in adult male rats. *Small* 9(9–10):1715–1720. doi:10.1002/sml.201201548
- Imam SZ, Zhou Q, Yamamoto A, Valente AJ, Ali SF, Bains M, Roberts JL, Kahle PJ et al (2011) Novel regulation of parkin function through c-Abl-mediated tyrosine phosphorylation: implications for Parkinson's disease. *J Neurosci* 31(1):157–163. doi:10.1523/JNEUROSCI.1833-10.2011
- Wang H, Joseph JA (1999) Quantifying cellular oxidative stress by dichlorofluorescein assay using microplate reader. *Free Radic Biol Med* 27(5–6):612–616
- Trickler WJ, Lantz SM, Schrand AM, Robinson BL, Newport GD, Schlager JJ, Paule MG, Slikker W et al (2012) Effects of copper nanoparticles on rat cerebral microvessel endothelial cells. *Nanomedicine (Lond)* 7(6):835–846. doi:10.2217/nmm.11.154
- Trickler WJ, Lantz SM, Murdock RC, Schrand AM, Robinson BL, Newport GD, Schlager JJ, Oldenburg SJ et al (2010) Silver nanoparticle induced blood–brain barrier inflammation and increased permeability in primary rat brain microvessel endothelial cells. *Toxicol Sci* 118(1):160–170. doi:10.1093/toxsci/kfq244
- Deng XL, He F, Peng J, Yang LF, Zhang CL, Xiang QL, Wu LW, Wang GL et al (2011) Influence of lipopolydisaccharide on the permeability of rat brain microvascular endothelial cells and the molecular mechanism. *Zhongguo Dang Dai Er Ke Za Zhi* 13(11):908–911
- Imam SZ, Trickler W, Kimura S, Binienda ZK, Paule MG, Slikker W Jr, Li S, Clark RA et al (2013) Neuroprotective efficacy of a new brain-penetrating C-Abl inhibitor in a murine parkinson's disease model. *PLoS One* 8(5), e65129. doi:10.1371/journal.pone.0065129
- Colvin VL (2003) The potential environmental impact of engineered nanomaterials. *Nat Biotechnol* 21(10):1166–1170. doi:10.1038/nbt875

25. Borm PJ, Muller-Schulte D (2006) Nanoparticles in drug delivery and environmental exposure: same size, same risks? *Nanomedicine (Lond)* 1(2):235–249. doi:10.2217/17435889.1.2.235
26. Borm P, Klaessig FC, Landry TD, Moudgil B, Pauluhn J, Thomas K, Trottier R, Wood S (2006) Research strategies for safety evaluation of nanomaterials, part V: role of dissolution in biological fate and effects of nanoscale particles. *Toxicol Sci* 90(1):23–32. doi:10.1093/toxsci/kfj084
27. Lewinski N, Colvin V, Drezek R (2008) Cytotoxicity of nanoparticles. *Small* 4(1):26–49. doi:10.1002/sml.200700595
28. Nel A, Xia T, Madler L, Li N (2006) Toxic potential of materials at the nanolevel. *Science* 311(5761):622–627. doi:10.1126/science.1114397
29. Xia T, Kovochich M, Brant J, Hotze M, Sempf J, Oberley T, Sioutas C, Yeh JI et al (2006) Comparison of the abilities of ambient and manufactured nanoparticles to induce cellular toxicity according to an oxidative stress paradigm. *Nano Lett* 6(8):1794–1807. doi:10.1021/nl061025k
30. Sharma HS, Hussain S, Schlager J, Ali SF, Sharma A (2010) Influence of nanoparticles on blood–brain barrier permeability and brain edema formation in rats. *Acta Neurochir Suppl* 106:359–364. doi:10.1007/978-3-211-98811-4_65
31. Calderon-Garciduenas L, Solt AC, Henriquez-Roldan C, Torres-Jardon R, Nuse B, Herritt L, Villarreal-Calderon R, Osnaya N et al (2008) Long-term air pollution exposure is associated with neuroinflammation, an altered innate immune response, disruption of the blood–brain barrier, ultrafine particulate deposition, and accumulation of amyloid beta-42 and alpha-synuclein in children and young adults. *Toxicol Pathol* 36(2):289–310. doi:10.1177/0192623307313011
32. Horn D, Fontanesi F, Barrientos A (2008) Exploring protein-protein interactions involving newly synthesized mitochondrial DNA-encoded proteins. *Methods Mol Biol* 457:125–139
33. Horn D, Al-Ali H, Barrientos A (2008) Cmc1p is a conserved mitochondrial twin CX9C protein involved in cytochrome c oxidase biogenesis. *Mol Cell Biol* 28(13):4354–4364. doi:10.1128/MCB.01920-07
34. Charles AL, Guilbert AS, Bouitbir J, Goette-Di Marco P, Enache I, Zoll J, Piquard F, Geny B (2011) Effect of postconditioning on mitochondrial dysfunction in experimental aortic cross-clamping. *Br J Surg* 98(4):511–516. doi:10.1002/bjs.7384
35. Ali SF, Binienda ZK, Imam SZ (2011) Molecular aspects of dopaminergic neurodegeneration: gene-environment interaction in parkin dysfunction. *Int J Environ Res Public Health* 8(12):4702–4713. doi:10.3390/ijerph8124702
36. Zhu MT, Wang Y, Feng WY, Wang B, Wang M, Ouyang H, Chai ZF (2010) Oxidative stress and apoptosis induced by iron oxide nanoparticles in cultured human umbilical endothelial cells. *J Nanosci Nanotechnol* 10(12):8584–8590
37. Karlsson HL, Cronholm P, Gustafsson J, Moller L (2008) Copper oxide nanoparticles are highly toxic: a comparison between metal oxide nanoparticles and carbon nanotubes. *Chem Res Toxicol* 21(9):1726–1732. doi:10.1021/tx800064j
38. Earnshaw WC, Martins LM, Kaufmann SH (1999) Mammalian caspases: structure, activation, substrates, and functions during apoptosis. *Annu Rev Biochem* 68:383–424. doi:10.1146/annurev.biochem.68.1.383
39. Earnshaw WC (1999) Apoptosis. A cellular poison cupboard. *Nature* 397(6718):387–389. doi:10.1038/17015
40. Alarifi S, Ali D, Alkahtani S, Alhader MS (2014) Iron oxide nanoparticles induce oxidative stress, DNA damage, and caspase activation in the human breast cancer cell line. *Biol Trace Elem Res* 159(1–3):416–424. doi:10.1007/s12011-014-9972-0
41. Alarifi S, Ali D, Alakhtani S, Al Suhaibani ES, Al-Qahtani AA (2014) Reactive oxygen species-mediated DNA damage and apoptosis in human skin epidermal cells after exposure to nickel nanoparticles. *Biol Trace Elem Res* 157(1):84–93. doi:10.1007/s12011-013-9871-9
42. Ahamed M, Alhadlaq HA, Alam J, Khan MA, Ali D, Alarafi S (2013) Iron oxide nanoparticle-induced oxidative stress and genotoxicity in human skin epithelial and lung epithelial cell lines. *Curr Pharm Des* 19(37):6681–6690
43. Thomsen LB, Linemann T, Pondman KM, Lichota J, Kim KS, Pieters RJ, Visser GM, Moos T (2013) Uptake and transport of superparamagnetic iron oxide nanoparticles through human brain capillary endothelial cells. *ACS Chem Neurosci* 4(10):1352–1360. doi:10.1021/cn400093z
44. Morales M, Root DH (2014) Glutamate neurons within the mid-brain dopamine regions. *Neuroscience* 282C:60–68. doi:10.1016/j.neuroscience.2014.05.032
45. Dringen R (2000) Glutathione metabolism and oxidative stress in neurodegeneration. *Eur J Biochem* 267(16):4903
46. Taranukhin AG, Taranukhina EY, Saransaari P, Podkletnova IM, Pelto-Huikko M, Oja SS (2010) Neuroprotection by taurine in ethanol-induced apoptosis in the developing cerebellum. *J Biomed Sci* 17(1):S12. doi:10.1186/1423-0127-17-S1-S12
47. Repetto MG, Ossani G, Monserrat AJ, Boveris A (2010) Oxidative damage: the biochemical mechanism of cellular injury and necrosis in choline deficiency. *Exp Mol Pathol* 88(1):143–149. doi:10.1016/j.yexmp.2009.11.002
48. van Domburg PH, ten Donkelaar HJ (1991) The human substantia nigra and ventral tegmental area. A neuroanatomical study with notes on aging and aging diseases. *Adv Anat Embryol Cell Biol* 121:1–132
49. Hastie T, Tibshirani R, Botstein D, Brown P (2001) Supervised harvesting of expression trees. *Genome Biol* 2 (1): RESEARCH0003